Behavior of cation vacancies in single-crystal and in thin-film $SrTiO_3$: The importance of strontium vacancies and their defect associates

U. N. Gries,[1] M. Kessel,[1] F. V. E. Hensling,[2] R. Dittmann,[2] M. Martin,[1] and R. A. De Souza[1,*]

[1]*Institute of Physical Chemistry, RWTH Aachen University, 52056 Aachen, Germany*

[2]*Peter-Gruenberg Institute 7, Forschungszentrum Juelich GmbH, 52425 Juelich, Germany*

(Received 21 September 2020; accepted 13 November 2020; published 14 December 2020)

Solid-state diffusion experiments were used to probe the behavior of cation vacancies in the perovskite oxide $SrTiO_3$. Two types of nominally undoped (effectively acceptor-doped) $SrTiO_3$ systems were studied: (1) single crystals and (2) epitaxial thin films with different Sr/Ti stoichiometries produced by pulsed laser deposition. As diffusion sources, thin films of the perovskite oxide $BaZrO_3$ were employed, and diffusion anneals were carried out in air at $1323 \leqslant T/\mathrm{K} \leqslant 1523$ for single crystals and at $1073 \leqslant T/\mathrm{K} \leqslant 1223$ for thin films. Sample analysis by means of time-of flight secondary ion mass spectrometry (ToF-SIMS) yielded diffusion coefficients of Ba and Zr in $SrTiO_3$ (D_{Ba} and D_{Zr}). Diffusion profiles in single-crystal samples showed the expected error-function form and yielded $D_{Ba} \approx D_{Zr}$ at each temperature, and hence, activation enthalpies of diffusion that are approximately the same, at (3.0 ± 0.4) eV and (2.8 ± 0.4) eV. Diffusion profiles in the thin-film samples were unexpectedly complex, showing multiple error-function features. They also yielded $D_{Ba} \approx D_{Zr}$ at each temperature, however, but no clear trend was found as a function of Sr/Ti ratio. Comparing results for the two systems, we conclude that the concentration of cation vacancies is orders of magnitude higher in our thin-film samples than in the single crystals. Our results also provide experimental evidence that oxygen vacancies, $v_O^{\bullet\bullet}$, can decrease the activation enthalpy of strontium-vacancy migration by forming $(v_O v_{Sr})^{\times}$ defect associates, and we derive an analytical model for the cation diffusivity as a function of temperature and defect concentrations.

DOI: 10.1103/PhysRevMaterials.4.123404

I. INTRODUCTION

Perovskite-type oxides of the general formula ABO_3 are dominated without exception by vacancy rather than by interstitial point defects, by virtue of the lattice's close-packed nature. Oxygen vacancies are the most common vacancy defects because of the relative ease with which such defects form and migrate. Their behavior in a wide variety of perovskite oxides has been investigated extensively [1–9], and accordingly an advanced level of understanding has been attained. Cation vacancies in perovskites have attracted far less attention being considered far less mobile, and being present, in general, at far lower concentrations. Their presence cannot be ignored, however. At sufficiently high temperatures, they become mobile, allowing various fundamental processes to occur, processes such as interdiffusion, grain growth, sintering, creep, segregation, and accumulation at extended defects, and the precipitation of second phases.

In the prototypical perovskite oxide $SrTiO_3$, oxygen vacancies form readily, both upon reduction of the oxide, and to charge compensate acceptor impurities, such as Mg^{2+}, Al^{3+}, or Fe^{3+}, that substitute for Ti^{4+} [9–14]. The high mobility of oxygen vacancies at elevated temperatures has been long appreciated [10,15–18]; less well known is that at room temperature their mobility is still sufficiently high to provide the dominant contribution to the conductivity [9,19–21]. The activation enthalpy of oxygen-vacancy migration is found from a variety of experimental [17,21–24] and theoretical methods [25–28] to be ca. 0.65 eV. Interactions between oxygen vacancies and acceptor dopants increase the effective activation enthalpy up to 0.86–1.1 eV [29,30].

Strontium vacancies are known to be present and mobile in $SrTiO_3$ at high temperatures, since they allow the SrO-partial Schottky equilibrium to become active, precipitating SrO as a second phase at the surface [31–33]. At low temperatures, strontium vacancies are frozen-in, constituting additional acceptor species that are compensated by oxygen vacancies. Quantitative, experimental studies of strontium diffusion in $SrTiO_3$ are, however, surprisingly rare. Activation enthalpies have been reported in only six studies [23,34–38] since the 1960s, and one of these values [34] probably refers to grain-boundary diffusion, and another [35] refers to a lower limit; both are not considered further here. The remaining studies report values for the activation enthalpy of strontium-vacancy migration in bulk $SrTiO_3$ in the range of 2.5 eV to 4.0 eV (see Fig. 1).

Computational studies of Sr migration by a vacancy mechanism appear to confirm a value at the upper end of this range. Density-functional-theory (DFT) calculations [39,40] predict 4.0 eV and 3.7 eV; empirical-pair-potentials (EPP) calculations [25,41–46], though showing, as expected, a larger range of values (from 2.5 eV to 5 eV), yield values around 4 eV in four different studies, each based on a different set of EPP [25,42,43,46].

*desouza@pc.rwth-aachen.de

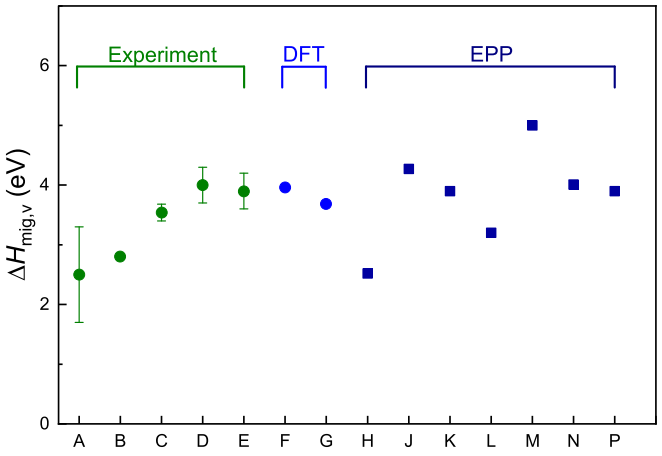

FIG. 1. Activation enthalpies of strontium-vacancy migration, $\Delta H_{mig,v}$, in $SrTiO_3$ reported in the literature from experiment (A [23], B [36], C [37], D [38], E [38]), from density-functional-theory (DFT) calculations (F [39], G [40]) and from empirical-pair-potential (EPP) calculations (H [41], J [42], K [43], L [44], M [45], N [25], P [46]).

On this basis, the lowest values obtained experimentally, of (2.5 ± 0.8) eV and 2.8 eV [23,36], would be attributed to experimental inaccuracy. There is, however, a computational prediction that suggests a closer examination is warranted. According to the DFT calculations of Walsh *et al.* [40], the presence of an oxygen vacancy directly adjacent to a strontium vacancy lowers the activation barrier for strontium-vacancy migration (in their calculations from 3.7 eV to 2.9 eV). Although this prediction accounts for the two lowest experimental values, some questions remain. For example, how reliable are these experimental values? One value [23] is characterized by a substantial error [(2.5 ± 0.8) eV], and the other [36] was obtained indirectly from transient impedance studies (and the associated error was not reported). The first aim of this study, therefore, is to obtain experimental diffusion data directly in order to examine the computational prediction. A second question is consequently under what conditions an activation enthalpy of $\approx$4 eV is observed and under what conditions an activation enthalpy of $\approx$3 eV. The second aim is, then, to construct a model, in order to identify the relevant conditions.

The third aim of this study is to extend the investigations from single-crystal samples to epitaxial thin-film samples. Thin films of $SrTiO_3$ often serve as a model system in studies of valence-change resistive switching [47], a phenomenon in which the resistance of an insulating oxide, after suitable preparation (a process called electroforming), can be switched reversibly between high and low resistance states upon application of suitable voltages. The mechanism of valence-change resistive switching is widely accepted to be a nanoscale redox reaction, brought about by the creation and migration of oxygen vacancies [48]. Three recent studies, however, have found evidence that strontium cations may also be mobile in these films during electroforming or switching processes [49–51]. For a deeper understanding of the resistive switching phenomenon, it is necessary, therefore, to characterize the behavior of cation defects in thin-film samples, behavior that is expected [52–54] to differ substantially from that in single crystal samples.

In particular, there is clear experimental evidence from positron annihilation lifetime spectroscopy (PALS) [52,55] that due to the nonequilibrium conditions of physical vapor deposition techniques, such as pulsed laser deposition (PLD), cation vacancies in state-of-the-art epitaxial oxide thin films are present in significant concentrations (i.e., much higher than their equilibrium concentration). The presence of cation vacancies in $SrTiO_3$ and other complex oxide thin films has not, however, received much attention in the community so far, although such defects have significant impact on electronic and ionic transport as well on functional properties such as magnetism and ferroelectricity [56]. In-depth studies on the role of cation vacancies are, therefore, of pivotal importance to advance the field of oxide electronics.

The experimental investigation of such slow-moving, minority defects is not easy. There are few techniques possessing the sensitivity to detect them. The most sensitive method for probing point-defect behavior, arguably, is a (tracer) diffusion experiment. Since diffusion in the solid state cannot occur without point defects, the observation of solid-state diffusion unambiguously indicates their presence (even defect concentrations orders of magnitude below the ppm level give rise to measurable diffusion coefficients [57]).

II. EXPERIMENTAL

A. Sample preparation and diffusion experiments

Nominally undoped, polished, (100) oriented single-crystal samples of $SrTiO_3$ were obtained commercially from CrysTec GmbH (Berlin, Germany). The samples measured 10 mm $\times$ 10 mm $\times$ 1 mm, and the polished large face exhibited an r.m.s. roughness of 2 nm, according to interference micrographs of an area of 425 μm $\times$ 920 μm (NT 1100, Veeco Instruments Inc., NY, USA). Samples were pre-annealed at the temperature of interest ($1323 \leqslant T/\mathrm{K} \leqslant 1523$) for a time (2–10)$t$ (t being the duration of the diffusion anneal), in order to equilibrate the cation sublattices. $BaZrO_3$ layers, approx. 200 nm thick, were deposited by PLD in an atmosphere of 10^{-2} mbar O_2 at room temperature (at IPC, RWTH Aachen University) and subsequently crystallized by annealing in air at $T = 973$ K for 4 hours.

Epitaxial thin films of $SrTiO_3$ with different Sr/Ti stoichiometries were grown by PLD (at PGI, Forschungszentrum Juelich) by varying the laser fluence [58,59]. Deposition took place at $T = 1073$ K onto single crystals of nominally undoped $SrTiO_3$ that had been etched with buffered HF solution according to the standard procedure [60,61] to yield TiO_2-terminated substrates. The different laser fluences used were 0.8 J cm^{-2} for Sr-rich films, 1.0 J cm^{-2} for stoichiometric films, and 1.2 J cm^{-2} for Ti-rich films. The target-substrate distance was 44 mm and the oxygen pressure during deposition, 0.1 mbar. Subsequently, the samples were cooled to $T = 673$ K, at which temperature thin films of $BaZrO_3$, approx. 10 nm thick, were deposited with a laser fluence of 1 J cm^{-2} at the same pressure and target-substrate distance and without exposing the $SrTiO_3$ thin films to air. No further

treatment of the sample was carried out to avoid substantial diffusion occurring before the diffusion anneal.

In previous studies [52,55,58], we have carefully analyzed $SrTiO_3$ thin films grown in this way by a variety of complementary characterization techniques [x-ray diffraction, x-ray photoelectron spectroscopy, PALS, and high resolution transmission electron microscopy (HRTEM)]. Based on these studies, we determined that both Sr and Ti vacancies are present for all Sr/Ti ratios, their relative concentration changing systematically with laser fluence [52,55]. It is important to note that for both stoichiometric and Ti-rich films HRTEM indicates high crystalline perfection without any extended defects such as Sr-vacancy platelets [62–64] or TiO_2 inclusions [65] that have been reported for Ti-rich films in the literature. For Sr-rich thin films, however, Ruddlesden-Popper type antiphase boundaries have been observed that accommodate the Sr surplus [55,66,67].

All prepared samples were cut into two pieces: One part was used for the diffusion experiment; the other was used as a zero-time reference. The diffusion anneals were carried out in air at $1323 \leqslant T/\mathrm{K} \leqslant 1523$ for the single crystals and at $1073 \leqslant T/\mathrm{K} \leqslant 1223$ for the thin films.

B. ToF-SIMS analysis

Diffusion profiles were determined by means of time-of-flight secondary ion mass spectrometry (ToF-SIMS) with a TOF-SIMS IV machine (IONTOF GmbH, Münster, Germany) [68]. Secondary ions for ToF analysis were generated by a pulsed beam of 25 keV Ga^+ rastered over 100 μm × 100 μm. A beam of 1 keV O_2^+ was used to sputter etch the sample over an area of 300 μm × 300 μm. To compensate the charge of the primary beams, a beam of low-energy (<20 eV) electrons was used. Positive secondary ions were recorded with a ToF cycle time of 55 μs. Crater depths were measured post-analysis with a profilometer (Dektak 150, Veeco Instruments Inc., NY, USA).

C. Profile description

Consideration of the diffusion experiments indicates that the initial and boundary conditions correspond to a thin source of extent h diffusing into a semi-infinite medium. The appropriate solution of the diffusion equation is thus [69]

$$I^{\mathrm{norm}}_{\mathrm{MO^+}}(x) = K\left[\mathrm{erf}\left(\frac{x+h}{\sqrt{4D_{\mathrm{cat}}t+4\sigma^2}}\right) - \mathrm{erf}\left(\frac{x-h}{\sqrt{4D_{\mathrm{cat}}t+4\sigma^2}}\right)\right], \quad (1)$$

where $I^{\mathrm{norm}}_{\mathrm{MO^+}}(x)$ is the secondary ion intensity of MO^+ relative to that of O^+ as a function of depth x, K is a fitting parameter, D_{cat} is the cation diffusion coefficient ($D^{\mathrm{sc}}_{\mathrm{cat}}$ for single crystals, $D^{\mathrm{tf}}_{\mathrm{cat}}$ for thin films), t is the duration of the diffusion anneal, and σ characterizes the effective SIMS depth resolution, which is determined by surface/interface roughness and ion beam mixing effects.

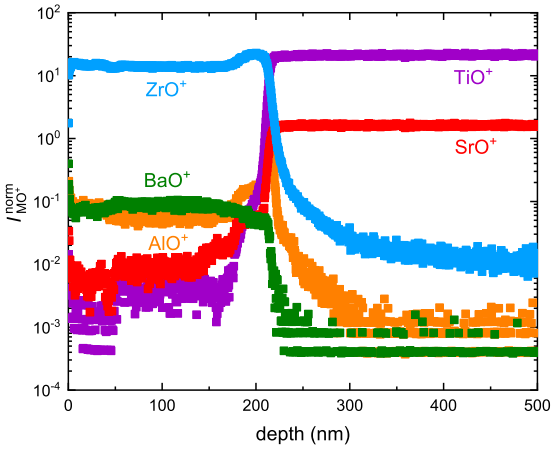

FIG. 2. Secondary ion intensities for MO^+ normalized to that of O^+ obtained by ToF-SIMS depth profiling of a $BaZrO_3|SrTiO_3$ sample prior to diffusion annealing (zero-time sample).

III. RESULTS

A. Single-crystal strontium titanate

The ToF-SIMS depth profile obtained for a sample after crystallization but before diffusion annealing is shown in Fig. 2. The depth scale was corrected for the slightly different sputter rates of $BaZrO_3$ and $SrTiO_3$. The sharp decreases in the normalized BaO^+ and ZrO^+ signals and the sharp increases in the normalized SrO^+ and TiO^+ signals indicate a well-defined film, with little mixing of the cations across the interface. As the interface is approached, $I^{\mathrm{norm}}_{\mathrm{ZrO^+}}$ increases slightly, while $I^{\mathrm{norm}}_{\mathrm{BaO^+}}$ decreases slightly. All samples showed such changes prior to annealing but not afterwards.

Also evident in Fig. 2 is that aluminium is present as an impurity certainly in the $BaZrO_3$ film ($I^{\mathrm{norm}}_{\mathrm{AlO^+}}$ being significantly above the detector-background level) and possibly in the $SrTiO_3$ substrate ($I^{\mathrm{norm}}_{\mathrm{AlO^+}}$ being approximately at detector background). There is also a sharp peak in $I^{\mathrm{norm}}_{\mathrm{AlO^+}}$ at the $BaZrO_3|SrTiO_3$ interface, which we attribute to polishing residues on the $SrTiO_3$ substrate. Sr and Ti are present as impurities in $BaZrO_3$. A significant amount of Zr is present in the single-crystal $SrTiO_3$.

Exemplary profiles before and after diffusion annealing are compared in Fig. 3. In order to determine $D^{\mathrm{sc}}_{\mathrm{cat}}$, we first fitted Eq. (1) to the data for $t = 0$ to obtain h and σ. For the data shown in Fig. 2(a), for example, we obtained $h = (268 \pm 1)$ nm and $\sigma = (4.1 \pm 0.9)$ nm; the relatively large value of the latter strongly suggests that surface/interface roughness determines the depth resolution rather than ion-beam mixing. Having obtained h and σ, we then fitted Eq. (1) to the diffusion profile to determine $D^{\mathrm{sc}}_{\mathrm{cat}}$. The diffusion profile data for both Ba and Zr are described well, over several orders of magnitude in intensity, down to the detection limit.

Values obtained for $D^{\mathrm{sc}}_{\mathrm{Ba}}$ and $D^{\mathrm{sc}}_{\mathrm{Zr}}$ are plotted in Fig. 4. They are seen to be the same, within error, at all temperatures. The activation enthalpies of diffusion are $\Delta H_{\mathrm{Ba}} = (3.0 \pm 0.4)$ eV and $\Delta H_{\mathrm{Zr}} = (2.8 \pm 0.4)$ eV.

B. Thin-film strontium titanate

The ToF-SIMS depth profile of the as-grown $BaZrO_3|SrTiO_3|SrTiO_3$ structure is shown in Fig. 5. The

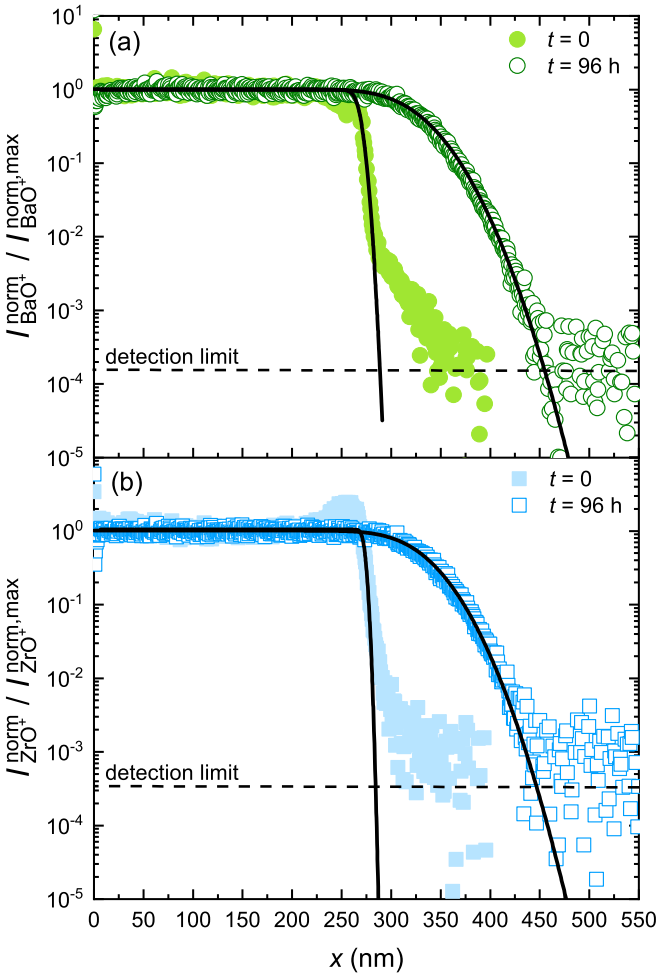

FIG. 3. Diffusion profiles in single-crystal strontium titanate after diffusion annealing for $t = 96$ h at $T = 1523$ K compared with zero-time profiles: (a) barium and (b) zirconium.

interface between the two thin films appears relatively sharp, with all signals dropping or rising abruptly (the ZrO^+ signal at low intensities decays over a longer length scale). As expected, the interface between thin-film $SrTiO_3$ and single-crystal $SrTiO_3$ is apparent neither in the matrix signals, $I^{\mathrm{norm}}_{SrO^+}$ and $I^{\mathrm{norm}}_{TiO^+}$, nor in the impurity signals, $I^{\mathrm{norm}}_{BaO^+}$ and $I^{\mathrm{norm}}_{ZrO^+}$. There is a peak in $I^{\mathrm{norm}}_{AlO^+}$ at a depth of ca. 100 nm, which we attribute, as before, to polishing residues on the $SrTiO_3$ substrate, and which thus indicates the extent of the $SrTiO_3$ thin film.

In Fig. 6 we compare diffusion profiles after a diffusion anneal of 20 h and then again after a further 45 h of annealing, with the zero-time profiles. The Ba diffusion profile after 20 h clearly shows two features, each of which has the error-function form of Eq. (1), but after 65 h only one feature is evident. In contrast, the Zr diffusion profile shows two features after 20 h and after 65 h. In general, the fits are not as good as for the single-crystal samples, but the normalised intensity can be described by the fitted curve over at least one order of magnitude (and in many cases, over two to four orders of magnitude). In some profiles, a third feature, just above background, is evident; since $\ln I^{\mathrm{norm}}$ seems to vary linearly with depth for this feature [70], we tentatively attribute it to

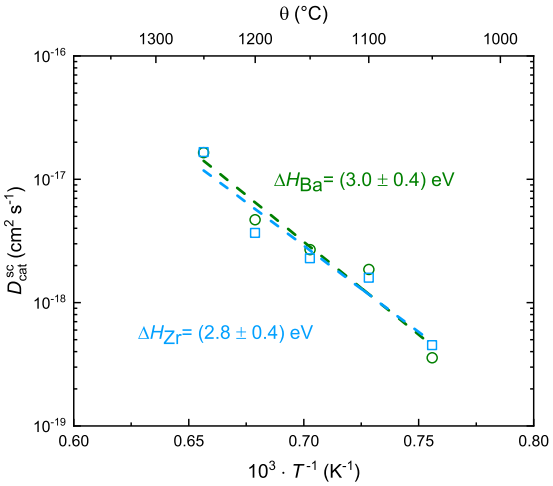

FIG. 4. Diffusion coefficients of barium (green circles) and zirconium (blue squares) in single-crystal strontium titanate as a function of inverse temperature.

fast diffusion of cations along dislocations. The poor signal-to-noise ratio for the data does not permit, however, definite identification, and we do not consider a possible third feature any further here.

Diffusion coefficients obtained for thin-film $STiO_3$ are plotted in Fig. 7. Again, one sees no difference between D_{Ba} and D_{Zr}. The two lines shown in the figure are not, however, fits to determine activation enthalpies. Rather the dashed line was calculated by taking $D^{\mathrm{sc}}_{\mathrm{cat}}(T)$ from Fig. 4, extrapolating it to lower temperatures, and multiplying it by 4000. This result strongly suggests that the thin-film samples have a factor of 4000 more cation vacancies than the single crystals, since the activation enthalpy of diffusion stays the same at $\Delta H_D \approx 3$ eV. The dotted line was obtained by fixing the activation enthalpy at $\Delta H_D = 4$ eV and varying the pre-exponential factor to describe the data.

In Fig. 8, we show the behavior of the faster cation diffusion process in thin-film $SrTiO_3$ as a function of Sr/Ti ratio.

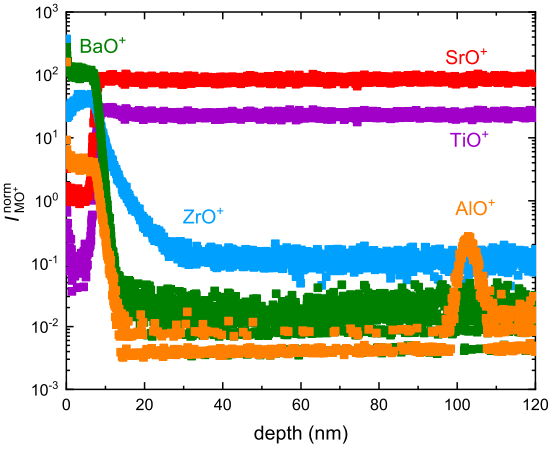

FIG. 5. Secondary ion intensities of MO^+ normalized to that of O^+ obtained by ToF-SIMS depth profiling for a $BaZrO_3|SrTiO_3|SrTiO_3$ sample prior to diffusion annealing (zero-time sample).

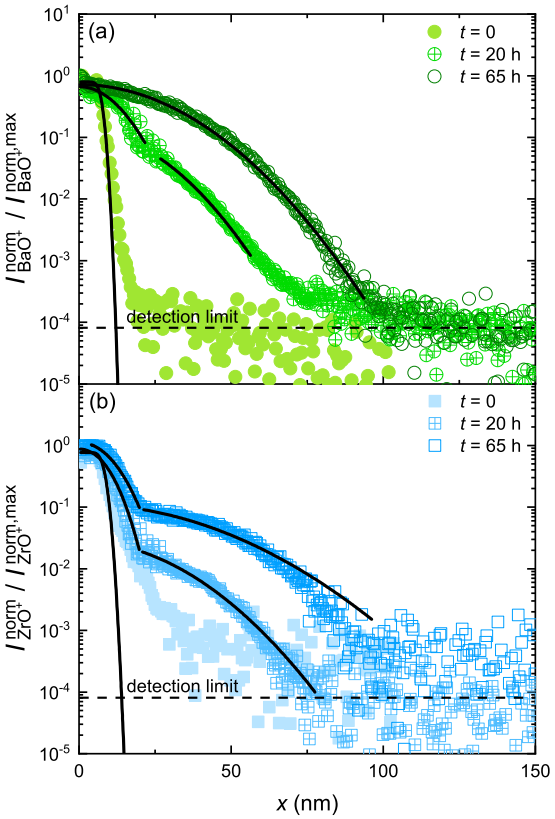

FIG. 6. Diffusion profiles in stoichiometric thin-film $SrTiO_3$ after diffusion anneals at $T = 1123$ K for various anneal times compared with the zero-time profile: (a) barium and (b) zirconium.

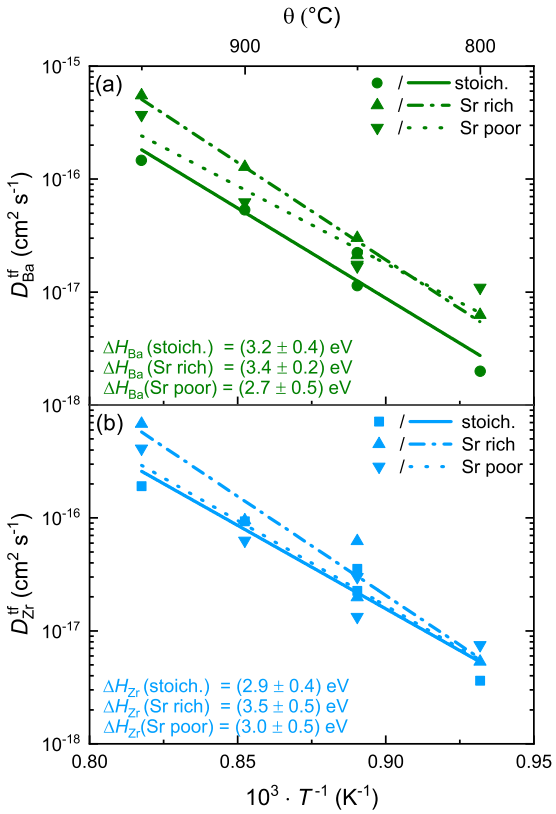

FIG. 8. Diffusion coefficients of Ba and Zr for the faster diffusion process in thin films of $SrTiO_3$ with differing Sr/Ti ratios as a function of inverse temperature.

Again, the behavior is far more complex than expected: As the composition of the $SrTiO_3$ film is changed from Sr-rich, through stoichiometric, to Ti-rich, the concentration of A-site vacancies is expected to increase monotonically and that of B-site vacancies to decrease monotonically. In Fig. 8, however, isothermal values of D^{tf}_{Ba} and D^{tf}_{Zr} are the lowest for the stoichiometric films. In general, D^{tf}_{Ba} and D^{tf}_{Zr} are the highest for the Sr-rich films.

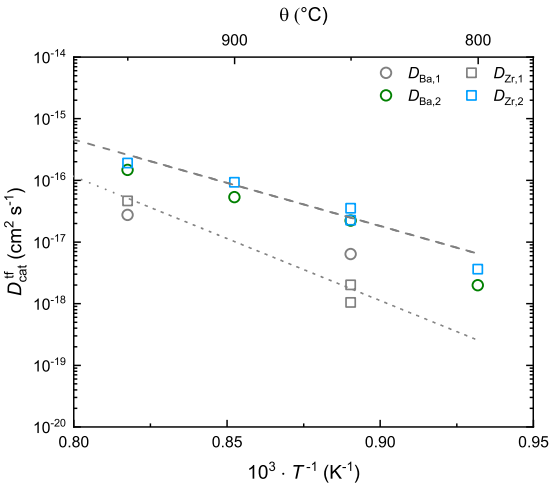

FIG. 7. Diffusion coefficients of barium and zirconium in stoichiometric thin-film $SrTiO_3$ as a function of inverse temperature. NB: Lines are not fits to Arrhenius behavior but (see text) descriptions with $\Delta H_D \approx 3$ eV (dashed line) and with $\Delta H_D \approx 4$ eV (dotted line).

IV. DISCUSSION

There are three major results obtained in this study concerning cation diffusion in perovskite $SrTiO_3$ to which we will pay special attention:

(i) $D_{Ba} \approx D_{Zr}$, with $\Delta H_{Ba} \approx \Delta H_{Zr}$ for both single-crystal and thin-film systems

(ii) the absolute magnitude of the activation enthalpy of diffusion and how this relates to the effect of oxygen vacancies on the migration of strontium vacancies

(iii) the differences between single-crystal and thin-film systems

A. A site vs B site

The sizes and environments of *A*-site and *B*-site cations in the ABO_3 perovskite structure differ substantially: The *A* cation is much larger than the *B* cation, and it is twelvefold coordinated by oxide ions, with the smaller *B* cation being sixfold coordinated by oxide ions. The charges of the two cations may also differ, as in $SrTiO_3$ or $NaNbO_3$, but not necessarily, as in $LaGaO_3$. Given these differing sizes, environments, and charges, it is surprising, therefore, to find $\Delta H_{Ba} \approx \Delta H_{Zr}$ for single-crystal (Fig. 4) and thin-film (Fig. 7) $SrTiO_3$.

Scrutiny of the literature reveals that such behavior is not specific to $SrTiO_3$. $\Delta H_A \approx \Delta H_B$ has been found previously for various ABO_3 perovskite compositions: $LaGaO_3$ [71], $BaTiO_3$ [72,73], $MgSiO_3$ [74–76], $BaZrO_3$ [77], (Ba,Sr)(Co,Fe)O_3 [78], and (La,Sr)FeO_3 [79]. Evidently, $\Delta H_A \approx \Delta H_B$ is characteristic of the ABO_3 structure.

Explanations for this behavior are also to be found in the literature. The specific details may vary, but all explanations require v_A to be present for v_B to migrate [71,77,80,81]. The issue, essentially, is the activation barrier for the migration of *B*-site cations being governed by repulsive Coulomb interactions between a migrating *B*-site cation and the *A*-site cations with which it comes into contact [80,81]. For a jump along ⟨110⟩, the migrating *B*-site cation comes into contact with two *A*-site cations; for a curved jump round the oxide-ion along ⟨100⟩, the migrating *B*-site cation comes into contact with one *A*-site cation, and if that *A*-site cation is removed, the *B*-site cation migrating along ⟨100⟩ comes into contact with no *A*-site cation. The corresponding activation barriers for vacancy migration decrease strongly in that order [80,81]. NB: experimental values of the activation enthalpy are generally in good agreement with calculated activation barriers for v_A migration. Monte Carlo calculations [82] with $(v_A v_B v_O)$ clusters that enable concerted diffusion of *A*-site and *B*-site cations [71] have shown that the ratio of diffusivities, D_A/D_B, will be around unity.

B. The activation enthalpy of cation diffusion in $SrTiO_3$

Comparing our results ($\Delta H_D \approx 3$ eV) with the experimental data plotted in Fig. 1, we find that our results are close to the two lowest experimental values (of 2.5 eV [23] and 2.8 eV [36]) rather than to the higher values of ≈4 eV [37,38]. In this way we confirm that a lower activation enthalpy is physically reasonable for cation diffusion in $SrTiO_3$. Furthermore, if we assume that the concentration of cation vacancies does not change as a function of temperature, so that $\Delta H_D \approx \Delta H_{\mathrm{mig,v}}$, our experiments confirm the prediction of Walsh *et al.* [40], that oxygen vacancies can lower the migration barrier for the migration of strontium vacancies.

Given, then, that two values are possible, $\Delta H_D \approx 4$ eV and $\Delta H_D \approx 3$ eV, it is important to know under what conditions each value will arise. We consider two factors to be important: the ratio of the defect concentrations, $[v''_{Sr}]$ to $[v^{\bullet\bullet}_O]$ and the temperature range of interest.

If there are many v''_{Sr} and few $v^{\bullet\bullet}_O$, most of the cation vacancies will be free, rather than in associates with oxygen vacancies, and the activation enthalpy will be around 4 eV. This is the case for donor-doped $SrTiO_3$ under oxidizing conditions and not excessively high temperatures [83], for which the electroneutrality condition is $[D^{\bullet}] = 2[v''_{Sr}] \gg 2[v^{\bullet\bullet}_O]$. In contrast, acceptor-doped $SrTiO_3$ is characterized under oxidizing conditions by $[A'] = 2[v^{\bullet\bullet}_O] \gg 2[v''_{Sr}]$; that is, there will be more than sufficient $v^{\bullet\bullet}_O$ present to form associates with v''_{Sr}, but the temperature has to be low enough for the associates to form.

Bearing this in mind, we now turn to the literature comparison in Fig. 9. Concentrating on the single-crystal datasets, we see that acceptor-doped systems [(a),(b),(d)] exhibit far lower $D^{\mathrm{sc}}_{\mathrm{cat}}$ than samples with high cation-vacancy concentrations

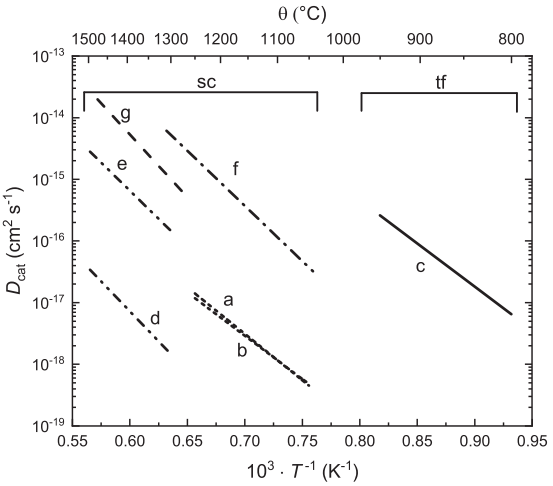

FIG. 9. Comparison of cation diffusion coefficients obtained for acceptor-doped and donor-doped $SrTiO_3$ as a function of inverse temperature for single-crystal (sc) and thin-film (tf) systems: (a), (b), (c) (this study); (d), (e), Ref. [38]; (f), Ref. [37]; (g), Ref. [84].

[(e),(f) being donor doped; (g) referring to Si diffusion in Si-implanted samples]. More importantly, we find that the latter datasets [(e),(f),(g)] have activation enthalpies of $\Delta H_D \approx 4$ eV, while the former acceptor-doped samples are characterized by $\Delta H_D \approx 4$ eV at high temperatures but $\Delta H_D \approx 3$ eV at lower temperatures. The observed behavior is thus qualitatively consistent with the proposed model.

It is instructive to take a further step and consider the behavior of an acceptor-doped system quantitatively. That is, we consider that cation diffusion occurs predominantly through individual strontium vacancies v''_{Sr} at higher temperatures, with diffusion coefficient D^{i}_{Sr}, and through strontium vacancies associated with oxygen vacancies, $(v_{Sr}v_O)^{\times}$, at lower temperatures, with diffusion coefficient D^{a}_{Sr}. The association reaction,

$$v''_{Sr} + v^{\bullet\bullet}_O \rightleftharpoons (v_{Sr}v_O)^{\times}, \tag{2}$$

is therefore required to lie on the left-hand side at higher temperatures and on the right-hand side at lower temperatures. Its equilibrium constant,

$$K_a(T) = \frac{[(v_{Sr}v_O)^{\times}]}{[v''_{Sr}][v^{\bullet\bullet}_O]} = K^0_a e^{-\Delta H_a/k_B T}, \tag{3}$$

is thus characterized by a negative enthalpy of association of, for example, $\Delta H_a = -1$ eV. Assuming the total amounts of strontium vacancies and oxygen vacancies to be constant within the crystal, one can calculate $[(v_{Sr}v_O)^{\times}]$ and $[v''_{Sr}]$ as a function of temperature [see Fig. 10(a)].

If one assumes that the associate can diffuse through the crystal without dissociating, the overall rate of Sr diffusion is then the sum of the two diffusion coefficients,

$$D_{Sr} = D^{\mathrm{i}}_{Sr} + D^{\mathrm{a}}_{Sr}. \tag{4}$$

Each diffusivity can be expressed as the product of that particular defect diffusivity and the site fraction of that defect,

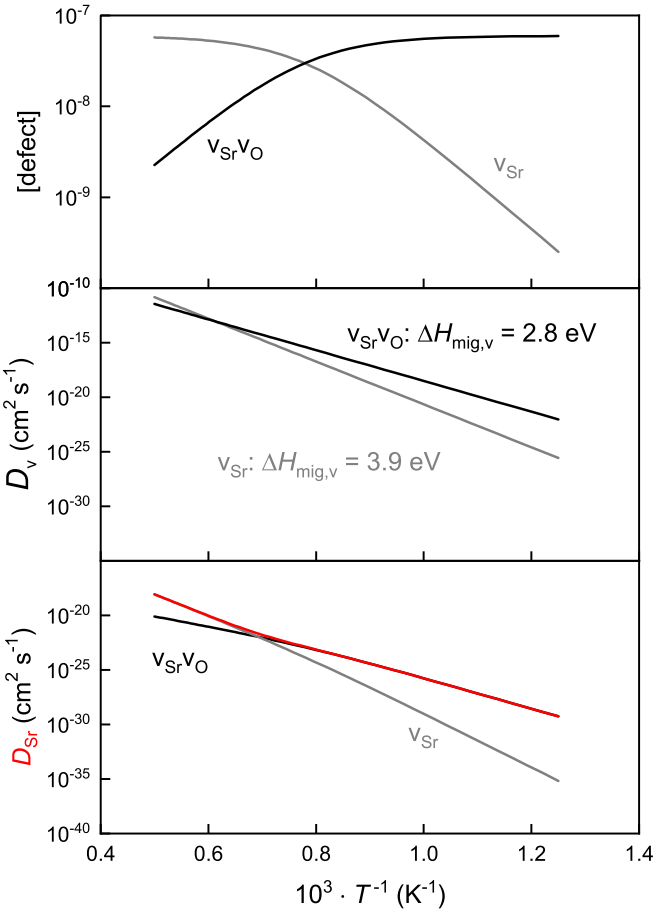

FIG. 10. (a) Concentration of isolated and associated strontium vacancies as a function of inverse temperature. (b) Defect diffusivities for isolated and associated strontium vacancies as a function of inverse temperature. (c) Individual and total strontium diffusivities as a function of inverse temperature. The total concentrations of strontium vacancies and oxygen vacancies are assumed to be constant.

$$D_{Sr} = D_{v^i}\frac{[v''_{Sr}]}{[Sr^{\times}_{Sr}]} + D_{v^a}\frac{[(v_{Sr}v_O)^{\times}]}{[Sr^{\times}_{Sr}]}. \quad (5)$$

$D_{v^i}(T)$ was calculated from experimental data [38] (see Ref. [85]); $D_{v^a}(T)$ is currently unknown, and so, values were chosen to produce effects in the temperature range of interest. Both defect diffusivities used as input in the model are shown in Fig. 10(b). Combining the data in Figs. 10(a) and 10(b), we obtain D_{Sr} plotted in Fig. 10(c).

Analysis of this data as a function of temperature reveals some interesting behavior. We calculated the activation enthalpy of strontium diffusion over a rolling interval of 60 K according to $\Delta H_D = -k_B(\partial \ln D_{Sr}/\partial T^{-1})$; the results are plotted in Fig. 11. This local activation enthalpy of Sr diffusion varies between 2.5 eV and 4 eV, for this assumed set of parameters, even though D_{v^i} and D_{v^a} have activation enthalpies of 3.9 eV and 2.9 eV. The more complex behavior comes from the changes in the respective defect concentrations with temperature.

Finally, in this section we note that the treatment so far has taken the total concentration of strontium vacancies to be

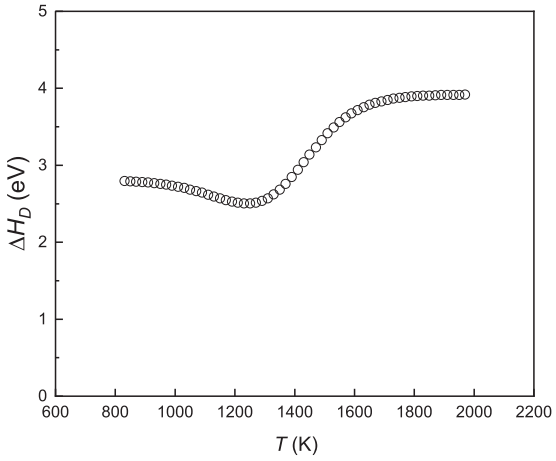

FIG. 11. Local activation enthalpy of strontium diffusion as a function of temperature obtained over a rolling interval of 60 K from the D_{Sr} data shown in Fig. 10(c).

constant. If the samples are in thermodynamic equilibrium, an additional term will contribute to the effective activation enthalpy of Sr diffusion, the enthalpy of vacancy generation (ΔH_{gen}) which reflects the increase in Sr-vacancy concentration with increasing temperature. If the $SrTiO_3$ sample is governed by $[A'] = 2[v^{\bullet\bullet}_O] \gg 2[v''_{Sr}]$, the additional term will be equal to the enthalpy of SrO-partial Schottky disorder ($\Delta H_{Sch} = 2.5$ eV [11]), whereas if SrO-partial Schottky disorder dominates the electroneutrality condition, $2[v''_{Sr}] = 2[v^{\bullet\bullet}_O]$, one finds $\Delta H_{gen} = \Delta H_{Sch}/2$. Thus, the effective activation enthalpy of Sr diffusion in acceptor-doped $SrTiO_3$ may take a variety of values, from 2.5 eV (see Fig. 11) up to 6.5 eV ($= \Delta H_{mig,v^i} + \Delta H_{Sch}$). There is no one value for the activation enthalpy of Sr diffusion in $SrTiO_3$.

C. Thin films versus single crystals

Examination of Fig. 9 emphasises that, despite the lower diffusion temperatures, the cation diffusion coefficients for the thin films are generally higher than those for the single crystals. This was attributed (see Sec. III B) to the increased concentrations of cation vacancies in PLD thin films, confirming results from earlier PALS studies [52,55]. In such thin-film systems, the concentrations of cation vacancies are determined by the deposition process, rather than by thermodynamics. Consequently, cation sublattices in thin-film samples are not in equilibrium, and their defect populations will vary according to the specific details of the deposition process.

The second point of interest is how D^{tf}_{cat} varies with the cation stoichiometry of the deposited films. A closer examination of Fig. 8 suggests that the Sr-rich films deviate from the expected behavior. They generally show the highest cation diffusion coefficients, but one would expect that they exhibit the lowest, since Sr-rich films have few v''_{Sr}, and such A-site vacancies are necessary for cation diffusion to take place (see Sec. IV A). One explanation for this discrepancy is the presence of Ruddlesden-Popper type antiphase boundaries in Sr-rich films. A recent study [86] on Sr-rich films has shown that such antiphase boundaries act as fast paths for

Sr diffusion relative to that in the $SrTiO_3$ lattice. As a consequence cation diffusion in such thin films is accelerated.

The third point of interest is appearance of two features in the cation diffusion profiles. Such behavior was not seen for the single crystal samples but only for the thin-film samples. We tentatively ascribe this to a significant change in sample composition: More Ba and Zr was incorporated into the thin-film samples, on account of the higher cation-vacancy concentration. As a consequence, cation diffusion takes place not in $SrTiO_3$ but in a $(Ba,Sr)(Zr,Ti)O_3$ solid solution. This would change the defect thermodynamics, leading to fewer cation vacancies associating with oxygen vacancies, and in this way, cation diffusion takes place more slowly and with a higher activation enthalpy.

V. CONCLUDING REMARKS

We have demonstrated the application of cation diffusion experiments in order to probe the behavior of minority, slow-moving cation vacancies in single-crystal and thin-film samples of perovskite $SrTiO_3$. Three points are emphasized.

Our results provide experimental evidence for Sr vacancies migrating either alone or as part of associates with oxygen vacancies. Such behavior adds a degree of complexity to the process of cation diffusion in $SrTiO_3$. Such behavior also emphasizes the difference between anion and cation transport in ABO_3 perovskites. Defect association reduces the diffusivity of oxygen vacancies and increases the activation enthalpy of oxygen transport [29]. In contrast, defect association increases the diffusivity of strontium vacancies and decreases the activation enthalpy of cation diffusion. This accords well with the hypothesis [25,85] that structural perturbations impede highly mobile ions in oxides but accelerate comparatively immobile ions.

Second, we confirm that epitaxial oxide thin films contain high concentrations of cation vacancies, well above equilibrium values, and we are able to quantify the difference relative to single-crystal samples. Such differences need to be taken into account when studying electronic and ionic transport in epitaxial thin films and heterostructures, since cation vacancies, as acceptor-type defects, introduce states into the band gap and interact strongly with oxygen vacancies. In addition, the high cation-vacancy concentrations combined with the higher mobility of $(v_{Sr}v_O)^\times$ associates lead to a comparatively high cation diffusivity at relatively low temperatures.

Third, our results allowed us to construct a model that quantitatively describes the complicated cation diffusion behavior as a function of temperature and defect concentration. The model indicates that the effective activation enthalpy of cation diffusion in $SrTiO_3$ can take values from 2.5 eV up to 6.5 eV, depending on the temperature and whether the total concentration of cation defects varies with temperature or not. In this way it provides quantitative data that will aid in the interpretation of fundamental processes (dislocation climb [87], sintering [88,89], grain growth [89–91], and creep [92–94]) that involve the diffusion of cation vacancies.

ACKNOWLEDGMENTS

Funding from German Research Foundation (DFG) within the framework of the collaborative research center SFB917, "Nanoswitches," is acknowledged.

[1] T. Ishigaki, S. Yamauchi, K. Kishio, J. Mizusaki, and K. Fueki, J. Solid State Chem. **73**, 179 (1988).
[2] J. Mizusaki, Solid State Ionics **52**, 79 (1992).
[3] J. B. Goodenough, Ann. Rev. Mater. Res. **33**, 91 (2003).
[4] J. A. Kilner, A. Berenov, and J. Rossiny, in *Perovskite Oxide for Solid Oxide Fuel Cells*, edited by T. Ishihara (Springer US, Boston, MA, 2009), pp. 95–116.
[5] M. Cherry, M. Islam, and C. Catlow, J. Solid State Chem. **118**, 125 (1995).
[6] M. S. Islam, J. Mater. Chem. **10**, 1027 (2000).
[7] J. A. Kilner, Solid State Ionics **129**, 13 (2000).
[8] T. T. Mayeshiba and D. D. Morgan, Solid State Ionics **296**, 71 (2016).
[9] R. A. De Souza, Adv. Funct. Mater. **25**, 6326 (2015).
[10] N.-H. Chan, R. K. Sharma, and D. M. Smyth, J. Electrochem. Soc. **128**, 1762 (1981).
[11] R. Moos and K. H. Härdtl, J. Am. Ceram. Soc. **80**, 2549 (1997).
[12] I. Denk, W. Münch, and J. Maier, J. Am. Ceram. Soc. **78**, 3265 (1995).
[13] R. A. De Souza, J. Fleig, R. Merkle, and J. Maier, Z. Metallkunde **94**, 218 (2003).
[14] T. Shi, Y. Chen, and X. Guo, Prog. Mater. Sci. **80**, 77 (2016).
[15] A. E. Paladino, L. G. Rubin, and J. S. Waugh, J. Chem. Phys. Solids **26**, 391 (1965).
[16] L. Walters and R. Grace, J. Phys. Chem. Solids **28**, 245 (1967).
[17] D. B. Schwarz and H. U. Anderson, J. Electrochem. Soc. **122**, 707 (1975).
[18] J. C. Amante, J. D. Crawley, J. Kim, and T. R. Lemberger, in *Point Defects and Related Properties of Ceramics, Ceramic Trans*, edited by T. Mason and J. L. Routbort (American Ceramics Society, Westerville, OH, 1991), pp. 303–312.
[19] R. A. De Souza and A. H. H. Ramadan, Phys. Chem. Chem. Phys. **15**, 4505 (2013).
[20] R. Waser, J. Am. Ceram. Soc. **74**, 1934 (1991).
[21] R. A. Maier and C. A. Randall, J. Am. Ceram. Soc. **99**, 3350 (2016).
[22] F. Cordero, Phys. Rev. B **76**, 172106 (2007).
[23] A. Hackmann and O. Kanert, Radiat. Eff. Defects Solids **119-121**, 651 (1991).
[24] R. A. De Souza, V. Metlenko, D. Park, and T. E. Weirich, Phys. Rev. B **85**, 174109 (2012).
[25] V. Metlenko, A. Ramadan, F. Gunkel, H. Du, H. Schraknepper, S. Hoffmann-Eifert, R. Dittmann, R. Waser, and R. A. De Souza, Nanoscale **6**, 12864 (2014).
[26] S. P. Waldow and R. A. De Souza, ACS Appl. Mater. Interf. **8**, 12246 (2016).
[27] L. Zhang, B. Liu, H. Zhuang, P. Kent, V. R. Cooper, P. Ganesh, and H. Xu, Comput. Mater. Sci. **118**, 309 (2016).
[28] M. Lontsi-Fomena, A. Villesuzanne, J.-P. Doumerc, C. Frayret, and M. Pouchard, Comput. Mater. Sci. **44**, 53 (2008).

[29] M. Schie, R. Waser, and R. A. De Souza, J. Phys. Chem. C **118**, 15185 (2014).

[30] V. Metlenko, W. Jung, S. R. Bishop, H. L. Tuller, and R. A. De Souza, Phys. Chem. Chem. Phys. **18**, 29495 (2016).

[31] Y. Liang and D. A. Bonnell, Surf. Sci. **285**, L510 (1993).

[32] B. Rahmati, J. Fleig, W. Sigle, E. Bischoff, J. Maier, and M. Rühle, Surf. Sci. **595**, 115 (2005).

[33] R. Meyer, R. Waser, J. Helmbold, and G. Borchardt, J. Electroceram. **9**, 101 (2002).

[34] P. Turlier, P. Bussiere, and M. Prettre, C. R. Hebd. Seances Acad. Sci. **250**, 1649 (1960).

[35] W. H. Rhodes and W. D. Kingery, J. Am. Ceram. Soc. **49**, 521 (1966).

[36] F. Poignant and P. Abelard, Radiat. Eff. Defects Solids **151**, 103 (1999).

[37] R. Meyer, R. Waser, J. Helmbold, and G. Borchardt, Phys. Rev. Lett. **90**, 105901 (2003).

[38] K. Gomann, G. Borchardt, M. Schulz, A. Gomann, W. Maus-Friedrichs, B. Lesage, O. Kaitasov, S. Hoffmann-Eifert, and T. Schneller, Phys. Chem. Chem. Phys. **7**, 2053 (2005).

[39] T. Mizoguchi, N. Takahashi, and H.-S. Lee, Appl. Phys. Lett. **98**, 091909 (2011).

[40] A. Walsh, C. R. A. Catlow, A. G. H. Smith, A. A. Sokol, and S. M. Woodley, Phys. Rev. B **83**, 220301(R) (2011).

[41] M. J. Akhtar, Z.-U.-N. Akhtar, R. A. Jackson, and C. R. A. Catlow, J. Am. Ceram. Soc. **78**, 421 (1995).

[42] J. Crawford and P. Jacobs, J. Solid State Chem. **144**, 423 (1999).

[43] B. Thomas, N. Marks, and B. Begg, Nucl. Instrum. Methods Phys. Res., Sec. B **254**, 211 (2007).

[44] C. R. A. Catlow, Z. X. Guo, M. Miskufova, S. A. Shevlin, A. G. H. Smith, A. A. Sokol, A. Walsh, D. J. Wilson, and S. M. Woodley, Philos. Trans. R. Soc., A **368**, 3379 (2010).

[45] B. P. Uberuaga and L. J. Vernon, Solid State Ionics **253**, 18 (2013).

[46] R. E. Ward, C. L. Freeman, J. S. Dean, D. C. Sinclair, and J. H. Harding, Adv. Funct. Mater. **30**, 1905077 (2020).

[47] C. Baeumer, C. Schmitz, A. H. H. Ramadan, H. Du, K. Skaja, V. Feyer, P. Müller, B. Arndt, C.-L. Jia, J. Mayer, R. A. De Souza, C. M. Schneider, R. Waser, and R. Dittmann, Nat. Commun. **6**, 8610 (2015).

[48] R. Waser and M. Aono, Nat. Mater. **6**, 833 (2007).

[49] C. Lenser, A. Koehl, I. Slipukhina, H. Du, M. Patt, V. Feyer, C. M. Schneider, M. Lezaic, R. Waser, and R. Dittmann, Adv. Funct. Mater. **25**, 6360 (2015).

[50] H. Du, C.-L. Jia, A. Koehl, J. Barthel, R. Dittmann, R. Waser, and J. Mayer, Chem. Mater. **29**, 3164 (2017).

[51] D.-H. Kwon, S. Lee, C. S. Kang, Y. S. Choi, S. J. Kang, H. L. Cho, W. Sohn, J. Jo, S.-Y. Lee, K. H. Oh, T. W. Noh, R. A. De Souza, M. Martin, and M. Kim, Adv. Mater. **31**, 1901322 (2019).

[52] D. J. Keeble, S. Wicklein, R. Dittmann, L. Ravelli, R. A. Mackie, and W. Egger, Phys. Rev. Lett. **105**, 226102 (2010).

[53] R. A. De Souza, F. Gunkel, S. Hoffmann-Eifert, and R. Dittmann, Phys. Rev. B **89**, 241401(R) (2014).

[54] J. Zhu, J.-W. Lee, H. Lee, L. Xie, X. Pan, R. A. De Souza, C.-B. Eom, and S. S. Nonnenmann, Sci. Adv. **5**, eaau8467 (2019).

[55] D. J. Keeble, S. Wicklein, L. Jin, C. L. Jia, W. Egger, and R. Dittmann, Phys. Rev. B **87**, 195409 (2013).

[56] R. Dittmann, in *Epitaxial Growth of Complex Metal Oxides*, Woodhead Publishing Series in Electronic and Optical Materials, edited by G. Koster, M. Huijben, and G. Rijnders (Woodhead Publishing, Sawston, Cambridge, UK, 2015), pp. 231–261.

[57] M. P. Mueller, K. Pingen, A. Hardtdegen, S. Aussen, A. Kindsmueller, S. Hoffmann-Eifert, and R. A. De Souza, APL Mater. **8**, 081104 (2020).

[58] S. Wicklein, A. Sambri, S. Amoruso, X. Wang, R. Bruzzese, A. Koehl, and R. Dittmann, Appl. Phys. Lett. **101**, 131601 (2012).

[59] C. Xu, S. Wicklein, A. Sambri, S. Amoruso, M. Moors, and R. Dittmann, J. Phys. D: Appl. Phys. **47**, 034009 (2013).

[60] M. Kawasaki, K. Takahashi, T. Maeda, R. Tsuchiya, M. Shinohara, O. Ishiyama, T. Yonezawa, M. Yoshimoto, and H. Koinuma, Science **266**, 1540 (1994).

[61] G. Koster, G. Rijnders, D. H. Blank, and H. Rogalla, Physica C **339**, 215 (2000).

[62] T. Ohnishi, K. Shibuya, T. Yamamoto, and M. Lippmaa, J. Appl. Phys. **103**, 103703 (2008).

[63] Y. Tokuda, S. Kobayashi, T. Ohnishi, T. Mizoguchi, N. Shibata, Y. Ikuhara, and T. Yamamoto, Appl. Phys. Lett. **99**, 033110 (2011).

[64] C. M. Brooks, L. F. Kourkoutis, T. Heeg, J. Schubert, D. A. Muller, and D. G. Schlom, Appl. Phys. Lett. **94**, 162905 (2009).

[65] T. Suzuki, Y. Nishi, and M. Fujimoto, Phil. Mag. A **80**, 621 (2000).

[66] C. Xu, H. Du, A. J. H. van der Torren, J. Aarts, C.-L. Jia, and R. Dittmann, Sci. Rep. **6**, 38296 (2016).

[67] Y. Tokuda, S. Kobayashi, T. Ohnishi, T. Mizoguchi, N. Shibata, Y. Ikuhara, and T. Yamamoto, Appl. Phys. Lett. **99**, 173109 (2011).

[68] R. A. De Souza and M. Martin, MRS Bull. **34**, 907 (2009).

[69] J. Crank, *The Mathematics of Diffusion*, 2nd ed. (Oxford University Press, Oxford, 1975).

[70] A. D. Le Claire and A. Rabinovitch, J. Phys. C: Solid State Phys. **14**, 3863 (1981).

[71] O. Schulz, M. Martin, C. Argirusis, and G. Borchardt, Phys. Chem. Chem. Phys. **5**, 2308 (2003).

[72] S. Körfer, R. A. De Souza, H.-I. Yoo, and M. Martin, Solid State Sci. **10**, 725 (2008).

[73] H.-I. Yoo, C.-E. Lee, R. A. De Souza, and M. Martin, Appl. Phys. Lett. **92**, 252103 (2008).

[74] D. Yamazaki, T. Kato, H. Yurimoto, E. Ohtani, and M. Toriumi, Phys. Earth Planet. Inter. **119**, 299 (2000).

[75] C. Holzapfel, D. C. Rubie, D. J. Frost, and F. Langenhorst, Science **309**, 1707 (2005).

[76] J. Xu, D. Yamazaki, T. Katsura, X. Wu, P. Remmert, H. Yurimoto, and S. Chakraborty, J. Geophys. Res.: Solid Earth **116**, B12205 (2011).

[77] R. Sažinas, I. Sakaguchi, I. Hasle, J. M. Polfus, R. Haugsrud, M.-A. Einarsrud, and T. Grande, Phys. Chem. Chem. Phys. **19**, 21878 (2017).

[78] S. P. Harvey, R. A. De Souza, and M. Martin, Energy Environ. Sci. **5**, 5803 (2012).

[79] I. Wærnhus, N. Sakai, H. Yokokawa, T. Grande, M.-A. Einarsrud, and K. Wiik, Solid State Ionics **178**, 907 (2007).

[80] R. A. De Souza, M. S. Islam, and E. Ivers-Tiffee, J. Mater. Chem. **9**, 1621 (1999).

[81] R. A. De Souza and J. Maier, Phys. Chem. Chem. Phys. **5**, 740 (2003).

[82] I. V. Belova, G. E. Murch, D. Samuelis, and M. Martin, Defect Diffus. Forum **263**, 81 (2007).
[83] R. Meyer, A. F. Zurhelle, R. A. De Souza, R. Waser, and F. Gunkel, Phys. Rev. B **94**, 115408 (2016).
[84] I. Sakaguchi, S. Hishita, and H. Haneda, Nucl. Instrum. Methods Phys. Res., Sec. B **173**, 436 (2001).
[85] R. A. De Souza, in *Resistive Switching* (John Wiley & Sons, Ltd, Weinheim, Germany, 2016), Chap. 5, pp. 125–164.
[86] T. Heisig, J. Kler, H. Du, C. Baumer, F. Hensling, M. Glöß, M. Moors, A. Locatelli, T. O. Mentes, F. Genuzio, J. Mayer, R. A. De Souza, and R. Dittmann, Adv. Funct. Mater. **30**, 2004118 (2020).
[87] W. Sigle, C. Sarbu, D. Brunner, and M. Rühle, Philos. Mag. **86**, 4809 (2006).
[88] L. Amaral, A. M. Senos, and P. M. Vilarinho, Mater. Res. Bull. **44**, 263 (2009).
[89] F. Lemke, W. Rheinheimer, and M. J. Hoffmann, J. Ceram. Soc. Japan **124**, 346 (2016).
[90] S.-Y. Chung and S.-J. L. Kang, J. Am. Ceram. Soc. **83**, 2828 (2000).
[91] W. Rheinheimer and M. J. Hoffmann, Scr. Mater. **101**, 68 (2015).
[92] Z. Wang, S. Karato, and K. Fujino, Phys. Earth Planet. Inter. **79**, 299 (1993).
[93] S. Webb, I. Jackson, and J. Fitz Gerald, Phys. Earth Planet. Inter. **115**, 259 (1999).
[94] D. Singh, M. Lorenzo-Martíín, G. Chen, F. Gutiérrez-Mora, and J. Routbort, J. Eur. Ceram. Soc. **27**, 3377 (2007).